

---

This is an electronic reprint of the original article.  
This reprint may differ from the original in pagination and typographic detail.

Flajsman, Lukas; Wojewoda, Ondrej; Qin, Huajun; Davidkova, Kristyna; Urbánek, Michal; van Dijken, Sebastiaan

## Wideband Brillouin light scattering analysis of spin waves excited by a white-noise RF generator

*Published in:*  
Applied Physics Letters

*DOI:*  
[10.1063/5.0124764](https://doi.org/10.1063/5.0124764)

Published: 05/12/2022

*Document Version*  
Publisher's PDF, also known as Version of record

*Please cite the original version:*  
Flajsman, L., Wojewoda, O., Qin, H., Davidkova, K., Urbánek, M., & van Dijken, S. (2022). Wideband Brillouin light scattering analysis of spin waves excited by a white-noise RF generator. *Applied Physics Letters*, 121(23), Article 232402. <https://doi.org/10.1063/5.0124764>

---

This material is protected by copyright and other intellectual property rights, and duplication or sale of all or part of any of the repository collections is not permitted, except that material may be duplicated by you for your research use or educational purposes in electronic or print form. You must obtain permission for any other use. Electronic or print copies may not be offered, whether for sale or otherwise to anyone who is not an authorised user.

# Wideband Brillouin light scattering analysis of spin waves excited by a white-noise RF generator

Cite as: Appl. Phys. Lett. **121**, 232402 (2022); <https://doi.org/10.1063/5.0124764>

Submitted: 08 September 2022 • Accepted: 20 November 2022 • Published Online: 05 December 2022

 Lukáš Flajšman,  Ondřej Wojewoda,  Huajun Qin, et al.



View Online



Export Citation



CrossMark

## ARTICLES YOU MAY BE INTERESTED IN

[Spin Hall magnetoresistance in Pt/Y<sub>3</sub>Fe<sub>5</sub>O<sub>12</sub> bilayers grown on Si and Gd<sub>3</sub>Ga<sub>5</sub>O<sub>12</sub> substrates](#)

Applied Physics Letters **121**, 232403 (2022); <https://doi.org/10.1063/5.0124583>

[Nonequilibrium Casimir–Lifshitz friction force and anomalous radiation heating of a small particle](#)

Applied Physics Letters **121**, 231603 (2022); <https://doi.org/10.1063/5.0115748>

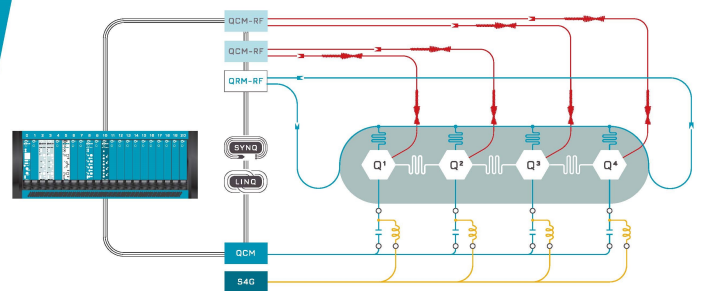
[A memristor based on two-dimensional MoSe<sub>2</sub>/MoS<sub>2</sub> heterojunction for synaptic device application](#)

Applied Physics Letters **121**, 233501 (2022); <https://doi.org/10.1063/5.0127880>

 QBLOX

Integrates all  
Instrumentation + Software  
for Control and Readout of  
**Superconducting Qubits**

[visit our website >](#)



# Wideband Brillouin light scattering analysis of spin waves excited by a white-noise RF generator

Cite as: Appl. Phys. Lett. **121**, 232402 (2022); doi: 10.1063/5.0124764

Submitted: 8 September 2022 · Accepted: 20 November 2022 ·

Published Online: 5 December 2022 · Publisher error corrected: 6 December 2022



View Online



Export Citation



CrossMark

Lukáš Flajšman,<sup>1,a)</sup> Ondřej Wojewoda,<sup>2</sup> Huajun Qin,<sup>3,4</sup> Kristýna Davidková,<sup>5</sup> Michal Urbánek,<sup>2,5</sup> and Sebastiaan van Dijken<sup>1</sup>

## AFFILIATIONS

<sup>1</sup>NanoSpin, Department of Applied Physics, Aalto University School of Science, P.O. Box 15100, FI-00076 Aalto, Finland

<sup>2</sup>CEITEC BUT, Brno University of Technology, 612 00 Brno, Czech Republic

<sup>3</sup>School of Physics and Technology, Wuhan University, Wuhan 430072, China

<sup>4</sup>Wuhan Institute of Quantum Technology, Wuhan 430206, China

<sup>5</sup>Institute of Physical Engineering, Brno University of Technology, 616 69 Brno, Czech Republic

<sup>a)</sup> Author to whom correspondence should be addressed: lukas.flajshman@aalto.fi

## ABSTRACT

Spin waves are studied intensively for their intriguing properties and potential use in future technology platforms for the transfer and processing of information and microwave signals. The characterization of devices and materials for magnonic systems is time-consuming, and thus, the development of instruments that can speed up the collection and analysis of spin-wave data is crucial. In this Letter, we report a straightforward approach to enhance the measurement throughput by fully exploiting the wideband detection nature of the Brillouin light scattering technique with a white-noise RF generator.

Published under an exclusive license by AIP Publishing. <https://doi.org/10.1063/5.0124764>

The Brillouin light scattering (BLS) technique has been used for decades as a tool to characterize the properties of spin waves or magnons (quanta of spin waves) in magnetic materials.<sup>1,2</sup> In micro-BLS,<sup>2</sup> inelastic scattering of photons on spin waves provides information on the spin-wave momentum, frequency, and phase with a spatial resolution of approximately 300 nm. The implementation of the BLS technique relies on precise spectrometers [scanning Fabry-Pérot<sup>2</sup> or more recently virtually imaged phase array (VIPA) spectrometers<sup>3</sup>] for the detection of minute changes in the scattered-light frequency with high contrast. Because BLS works in the frequency domain, it is capable of recording the entire spin-wave spectrum in a single-stage pass of the interferometer (Fabry-Pérot type spectrometer) or a single image (VIPA type spectrometer). BLS stands out from other spin-wave measurement techniques by its ability to detect non-coherent waves originating, e.g., from thermal<sup>4-6</sup> or spin-orbit-torque<sup>7</sup> excitations. Thermal excitation offers a truly wideband and flat spin-wave spectrum. The probing of thermal spin waves by BLS allows for the acquisition of full spin-wave spectra in a single measurement. Unfortunately, the low signal level<sup>8</sup> and non-directional excitation of thermal spin waves are incompatible with studies on the properties of

propagating spin waves in complex geometries, such as waveguides,<sup>9-12</sup> bends,<sup>13</sup> and resonators.<sup>14</sup> The intriguing frequency properties of these magnonic systems can be fully characterized by external excitation. This is conventionally done by connecting an RF generator to a microwave antenna fabricated on top of the sample and performing sweeps of successive single-frequency measurements.<sup>11-13</sup> The complete spectral response of the system is obtained by changing the RF frequency in a step-by-step fashion. For detailed spin-wave characterization, this requires PC-based automation, resulting in delays originating from synchronization issues and the non-optimal use of the spectrometer, as it scans over an extended frequency range while spin waves are excited only at a single frequency. The accumulation of these effects results in long measurement times.

Here, we introduce an approach for fast wideband BLS analysis of spin-wave properties. Integral to our method is the replacement of the RF generator by a white-noise RF source (Pasternack PE85N1012, see schematic in Fig. 1). In combination with a microwave antenna, the white-noise RF source provides wideband and directional excitation of propagating spin waves, thus combining the advantages of thermal and RF excitation while avoiding their drawbacks.

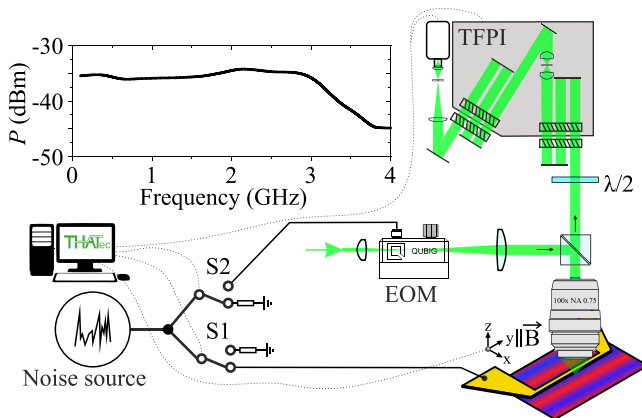


**FIG. 1.** A schematic of the BLS setup with optical and RF branches. After passing the electro-optical phase modulator (EOM, TW-15M1-VIS from QUBIG), the laser beam is split and focused on the sample by a microscope objective. The back-reflected light passes the half-wave plate (mounted in a rotational mount) before it enters the tandem Fabry-Pérot interferometer (TFPI, TFP-2 HC from Table Stable) for fine-spectrum analysis with high contrast. The RF signal from the noise source is split into two arms. Each arm contains a single microwave switch (S1 and S2). One branch connects to the microwave antenna fabricated on the sample, and the other feeds to the EOM. The graph in the top left corner shows a measurement of the total RF power provided by the white-noise source at 2 MHz measurement bandwidth.

We demonstrate the use of the white-noise RF generator in a commercial phase-resolved micro-focused BLS system (THATec Innovation GmbH). While the setup and measurement processes are simplified by replacing the RF generator with the white-noise source, we show that advanced studies including phase-resolved BLS<sup>15,16</sup> can still be performed. Because we excite and detect all frequencies within the noise source excitation range and BLS detection window simultaneously, we obtain large amounts of spin-wave data in a single measurement. The limiting factor of our approach is given by the frequency resolution of the spectrometer and the excitation bandwidth of the noise source. The signal of the white-noise source used in this work drops at around 3 GHz from  $-35$  to  $-45$  dBm (see graph in Fig. 1). The  $-45$  dBm signal is maintained up to about 12 GHz, where it drops further to  $-60$  dBm. The 3 GHz limit for efficient spin-wave excitation is given by the internal amplifier, while 12 GHz is the limit of the internal noise source. We note that noise sources with much higher bandwidths are readily available if one wishes to employ this BLS technique at higher frequency and that the excitation window can be tuned further by the use of an additional amplifier or bandpass filter.

We tested our approach by measuring the excitation and propagation of spin waves in a continuous liquid-phase-epitaxy (LPE) grown<sup>17</sup> 100-nm-thick yttrium iron garnet (YIG) film on a gadolinium gallium garnet (GGG) substrate. The spin waves are excited by a 500-nm-wide and 5  $\mu\text{m}$ -long microwave antenna with a 5 nm Ta/55 nm Au structure. The antenna is patterned by electron beam lithography and liftoff and connects to the white-noise source via a RF cable and RF probe.

In the first study, we positioned the BLS laser spot close to the center of the microwave antenna and swept the magnetic field (oriented along the microwave antenna) from 0 to 95 mT. For each value

of the external field, we recorded the BLS spectrum for two conditions: with the white-noise source off (S1 and S2 open) and with the white-noise source on (S1 closed, S2 open). All other parameters in the experiment were kept constant. The BLS intensity map recorded with the white-noise source on is shown in Fig. 2.

The BLS map shows two clear spin-wave branches. The bottom branch represents propagating Damon-Eshbach (DE) spin waves in the YIG film. The onset of this branch corresponds to the ferromagnetic resonance (FMR) frequency. The upper branch is the first perpendicular standing spin-wave (PSSW) mode. Comparing the BLS signal recorded with and without noise source (see the inset of Fig. 2 and the supplementary material, Fig. S1), we observe a well-resolved signal with high signal-to-noise ratio for active spin-wave excitation by the noise source and almost no signal when the noise source is disconnected (only thermal spin waves are measured). Because YIG is almost transparent at the BLS laser wavelength (532 nm), the back-scattering cross section of thermal spin waves is too small to be resolved.<sup>8</sup> Because we avoid delays stemming from synchronization, RF frequency sweeping, and the non-optimal use of the spectrometer, we are able to speed up the recording of the BLS intensity maps by about one order of magnitude compared to measurements with a single-tone RF generator for similar experimental parameters and signal-to-noise ratios.

To extract magnetic parameters, we fitted the maximum BLS signal in the two spin-wave branches using the Herring-Kittel formula.<sup>18</sup> Fits for the propagating spin waves and the PSSW mode are simultaneously performed to decorrelate the joint effect that some parameters have on the two branches. For a fixed parameter  $\gamma/2\pi = 28$  GHz/T, this analysis gives  $M_S = 148 \pm 2$  kA/m,  $A_{\text{ex}} = 3.64 \pm 0.1$  pJ/m,  $t = 96 \pm 3$  nm, and  $B_0 = 0.7 \pm 0.3$  mT for the saturation magnetization, exchange constant, film thickness, and effective anisotropy field, respectively. Information on the spin-wave dispersion can be obtained from the shape of the lower spin-wave band. However, this requires hard-to-find

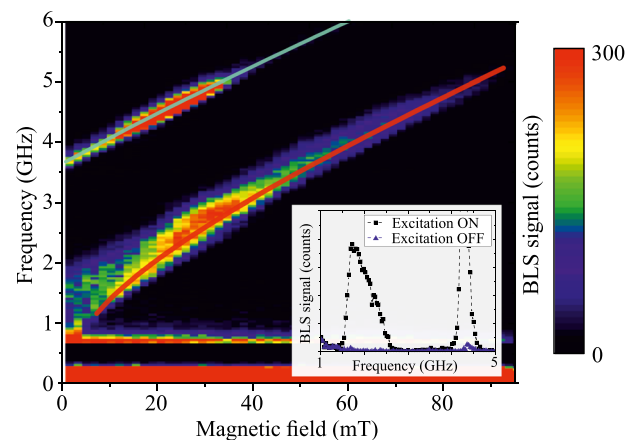


**FIG. 2.** BLS intensity map of excited spin-wave modes as a function of external magnetic field recorded with 2 mW laser power. Two main spin-wave branches are measured. The upper branch is the first perpendicular standing spin-wave mode, and the lower branch is the Damon-Eshbach mode. The lines are Levenberg-Marquardt fits of the Herring-Kittel formula<sup>18</sup> to the maximum signal of the individual branches. The inset shows single BLS spectra obtained at 10 mT with the white-noise source on (black squares) and off (blue triangles).

information on the spin-wave density of states, the excitation power factor of the antenna, and the BLS sensitivity factor.<sup>19,20</sup> Later, we will demonstrate a straightforward extraction of the spin-wave dispersion from phase-resolved BLS measurements with a white-noise source.

To further demonstrate the capabilities of our approach, we recorded spatial BLS intensity maps of the propagating spin waves [Fig. 3(a)]. In the experiments, we scanned the sample under the BLS laser spot in 300 nm steps while keeping the white-noise source on (S1 closed, S2 open). At each position, the BLS spectrum from 0 to 4.5 GHz is recorded. Because we excite and detect all modes simultaneously, it is possible to reconstruct (demultiplex) individual maps of propagating spin waves with a frequency step that is limited only by the setting of the spectrometer (50 MHz in our case). Selected maps are shown in Fig. 3(a). For a full set of spatial BLS intensity maps at different frequency, see the [supplementary material](#), Fig. S2.

The BLS maps show clear intensity signals that decay away from the microwave antenna. Well below the FMR frequency ( $\sim 1.9$  GHz), only direct excitation in the vicinity of the microwave antenna is measured [see BLS map for 1.5 GHz in Fig. 3(a)]. Starting at 1.7 GHz, caustic-like modes are emitted from the corners of the antenna [Fig. 3(a)]. Above the FMR frequency, the antenna also excites propagating DE spin waves. Because the microwave antenna is only 5  $\mu\text{m}$  long, interference of the caustic beams and the DE mode focuses the spin-wave intensity [see BLS map for 2.2 GHz in Fig. 3(a)], as previously observed in other works.<sup>21–23</sup> With increasing frequency, the focal point of spin-wave intensity moves closer to the microwave antenna. The 500-nm-wide antenna does not excite spin waves with a wavelength below  $\approx 700$  nm, leading to an abrupt drop in BLS intensity above 2.7 GHz (see the [supplementary material](#), Fig. S2). A BLS signal originating from the first PSSW mode is measured above 4 GHz [see BLS map for 4.2 GHz in Fig. 3(a)].

Wideband data collection during a single BLS scan can be used for high-throughput extraction of spin-wave parameters. As an example, we determine the frequency dependence of the spin-wave decay length. We do this by line-averaging the BLS signal in the rectangular area marked by white dashed lines in Fig. 3(a) and fitting the resulting line profiles to an exponentially decaying spin-wave intensity,<sup>24</sup>

$$I_{\text{SW}} = I_1 \exp\left(-\frac{2x}{\lambda_D}\right) + I_0. \quad (1)$$

Here,  $I_1$  is the initial spin-wave intensity,  $I_0$  is the background intensity originating from detector noise and thermal spin waves, and  $\lambda_D$  is the

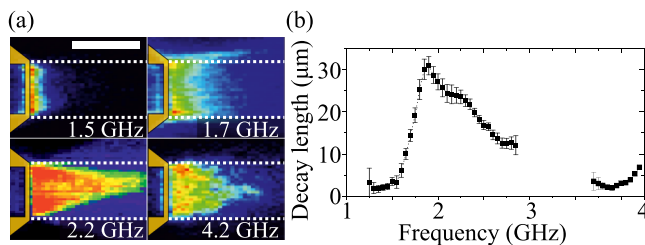


**FIG. 3.** (a) Spatial BLS intensity maps recorded at four frequencies, 17 mT external field, and 10 mW laser power. The microwave antenna is schematically overlaid on the maps. The scale bar in the top left panel indicates 5  $\mu\text{m}$ . The dotted lines mark the area from which we extracted data for further analysis. (b) Extracted spin-wave decay length as a function of frequency.

spin-wave decay length. Figure 3(b) summarizes the extracted spin-wave decay length. The initial increase in the decay length below the FMR frequency represents data for the caustic-like beams that are emitted from the corners of the microwave antenna. The maximum decay length is obtained near the FMR frequency. The subsequent decrease in the decay length is caused by a reduction of the Damon–Eshbach spin-wave group velocity with increasing frequency but also by stronger focusing of the spin-wave intensity at high frequency. We note that nonlinear interactions between simultaneously excited spin waves with different frequencies could also limit the spin-wave decay length. We assessed this possibility by conducting single-frequency BLS scans using a single-tone RF generator. Because the decay length derived from these experiments are similar ( $27.1 \pm 1.8$  and  $23 \pm 3 \mu\text{m}$  at 2 GHz for the measurement with the noise source and the single-tone generator, respectively), we conclude that nonlinear effects do not affect the BLS measurements much at the power of the noise source used in this work.

The unique potential of the BLS technique does not end with the spatial mapping of the spin-wave intensity. It has been shown before that the BLS method can be easily extended to the visualization of the spin-wave phase.<sup>2,15,16</sup> This is done by connecting an electro-optic modulator (EOM) to the same RF source. The EOM produces sidebands to the laser spectrum with a constant phase. Because the sidebands stemming from propagating spin waves depend on their phase, interference of the two signals can be exploited to extract the phase information. This concept, which is well understood for spin-wave excitation by single-tone RF generators, can be extended to our BLS technique with a white-noise RF source. For this to work, the optical signals from the EOM and sample must be mutually coherent. Similar to white-light interferometry, we achieved coherency in our setup by closely matching the lengths of the two RF signal paths. When this condition is met, phase-resolved spin-wave measurements can be conducted over a broad frequency range in a single spatial scan. To demonstrate this type of measurement, we first roughly matched the intensity of the spin-wave signal (S1 closed, S2 open) and the EOM signal (S1 open, S2 closed) by rotating the  $\lambda/2$  plate. After this, we activated both switches and scanned the sample over the same area as in Fig. 3. An example of a phase-resolved BLS map recorded with a white-noise source is shown in Fig. 4(a) (for a full set of images see the [supplementary material](#), Fig. S3). The phase-resolved map of propagating spin waves clearly shows the fringes produced by the interference of the EOM and BLS signals.

The wideband BLS technique introduced here captures detailed phase information on the complex wave pattern resulting from interference between the caustic-like beams and the DE spin waves. In addition to focusing of the spin-wave intensity, mode interference also significantly bends the spin-wave wavefront [Fig. 4(a)]. Despite the use of a short microwave antenna causing these effects, we now demonstrate that single-scan BLS data collection with the white-noise source enables fast measurements of the spin-wave dispersion. Figure 4(b) shows the frequency dependence of the line-averaged phase-resolved BLS signal, which we derived from BLS maps like the one depicted in Fig. 4(a) by averaging the signal over the area marked by the white dashed lines. Focusing on the excitation of DE spin waves at frequencies ranging from 1.9 to 3.0 GHz, we observe a decreasing wavelength with increasing frequency. The data in Fig. 4(b) also reveal a well-defined phase relation with an almost constant initial offset at all

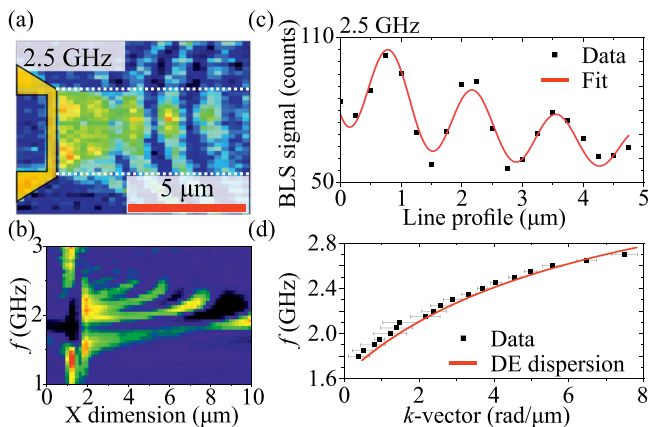


**FIG. 4.** (a) Phase-resolved BLS map recorded at 2.5 GHz, 17 mT external field, and 10 mW laser power. The microwave antenna is illustrated in yellow and the white dotted lines mark the area used for data extraction. (b) A map of spin-wave line profiles as a function of frequency. (c) Spin-wave line profile at 2.5 GHz and fit to the data. (d) Measured spin-wave dispersion and the calculated dispersion of DE spin waves in the YIG film.

frequencies. We fit the spin-wave profiles of individual frequency bins by a two-wave interference model,

$$I = I_{\text{SW}} + I_{\text{EOM}} + 2\sqrt{I_{\text{EOM}}I_{\text{SW}}} \cos\left(2\pi\frac{x}{\lambda} + \theta_0\right), \quad (2)$$

where  $\lambda$  is the spin-wave wavelength and  $\theta_0$  represents the initial phase offset between the EOM and the spin-wave signal. As an example, we show the experimental line profile measured at 2.5 GHz and a model fit in Fig. 4(c). The derived wave vector ( $k = 2\pi/\lambda$ ) is plotted for different excitation frequencies in Fig. 4(d) together with an analytical calculation of the DE spin-wave dispersion in the YIG film based on the magnetic parameters extracted previously ( $M_S$ ,  $A_{\text{ex}}$ ,  $t$ , and  $B_0$ ).<sup>25,26</sup> The good fit to the experimental data without any tuning of the magnetic parameters demonstrates the power of our high-throughput BLS measurement technique.

In summary, we present a twist to the well-established field of BLS-based spin-wave characterization. By replacing the single-tone RF generator with a relatively cheap wideband white-noise RF source, we reduce the measurement time by exciting and detecting full spectra of spin waves in a single BLS scan. We demonstrate the potential of the method by analyzing the field dependence of spin-wave modes and recording BLS maps of the spin-wave intensity and phase. The frequency resolution of the method, which is limited by the spectrometer, allows for fast measurements of the spin-wave dispersion relation. With these promising characteristics, we are confident that BLS setups with an integrated white-noise RF source will become a popular technique for high-throughput measurements of spin-wave properties.

See the [supplementary material](#) for BLS intensity maps as a function of external magnetic field recorded without excitation by the white-noise source (Fig. S1), a full set of spatial BLS intensity maps (Fig. S2), and a full set of phase-resolved BLS maps (Fig. S3).

This work was supported by the Academy of Finland (Grant Nos. 338748 and 325480). The authors acknowledge CzechNanoLab

Research Infrastructure supported by MEYS CR (No. LM2018110). O.W. was supported by Brno Ph.D. talent scholarship; the authors also acknowledge support from the project Quality Internal Grants of BUT (KInG BUT), Reg. No. CZ.02.2.69/0.0/0.0/19073/0016948, which is financed from the OP RDE and EF19\_073/0016948. The authors greatly appreciate the provision of the YIG samples by Carsten Dubs, INNOVENT e.V. Technologieentwicklung Jena.

## AUTHOR DECLARATIONS

### Conflict of Interest

The authors have no conflicts to disclose.

## Author Contributions

**Lukas Flajsman:** Investigation (equal); Methodology (equal); Visualization (lead); Writing – original draft (lead); Writing – review & editing (equal). **Ondřej Wojewoda:** Investigation (equal); Methodology (equal); Writing – review & editing (equal). **Huajun Qin:** Funding acquisition (lead). **Kristýna Davidková:** Resources (supporting). **Michal Urbánek:** Conceptualization (equal); Methodology (equal); Writing – review & editing (equal). **Sebastian van Dijken:** Funding acquisition (equal); Project administration (lead); Supervision (lead); Writing – review & editing (lead).

## DATA AVAILABILITY

The data that support the findings of this study are available from the corresponding author upon reasonable request.

## REFERENCES

- B. Hillebrands, “Progress in multipass tandem Fabry–Perot interferometry: I. A fully automated, easy to use, self-aligning spectrometer with increased stability and flexibility,” *Rev. Sci. Instrum.* **70**, 1589–1598 (1999).
- T. Sebastian, K. Schultheiss, B. Obry, B. Hillebrands, and H. Schultheiss, “Micro-focused Brillouin light scattering: Imaging spin waves at the nanoscale,” *Front. Phys.* **3**, 35 (2015).
- G. Yan, A. Bazir, J. Margueritat, and T. Dehoux, “Evaluation of commercial virtually imaged phase array and Fabry–Pérot based Brillouin spectrometers for applications to biology,” *Biomed. Opt. Express* **11**, 6933 (2020).
- J. Sandercock and W. Wetling, “Light scattering from thermal magnons in iron and nickel,” *IEEE Trans. Magn.* **14**, 442–444 (1978).
- B. Hillebrands, P. Baumgart, and G. Güntherodt, “*In situ* Brillouin scattering from surface-anisotropy-dominated Damon-Eshbach modes in ultrathin epitaxial Fe(110) layers,” *Phys. Rev. B* **36**, 2450–2453 (1987).
- J. F. Cochran and J. R. Dutcher, “Light scattering from thermal magnons in thin metallic ferromagnetic films,” *J. Appl. Phys.* **63**, 3814–3816 (1988).
- B. Divinskiy, V. E. Demidov, S. Urazhdin, R. Freeman, A. B. Rinkevich, and S. O. Demokritov, “Excitation and amplification of spin waves by spin-orbit torque,” *Adv. Mater.* **30**, 1802837 (2018).
- T. Hache, M. Vaňatka, L. Flajsman, T. Weinhold, T. Hula, O. Ciubotariu, M. Albrecht, B. Arkook, I. Barsukov, L. Fallarino, O. Hellwig, J. Fassbender, M. Urbánek, and H. Schultheiss, “Freestanding positionable microwave-antenna device for magneto-optical spectroscopy experiments,” *Phys. Rev. Appl.* **13**, 054009 (2020).
- V. E. Demidov, S. O. Demokritov, K. Rott, P. Krzysteczko, and G. Reiss, “Nano-optics with spin waves at microwave frequencies,” *Appl. Phys. Lett.* **92**, 232503 (2008).
- V. E. Demidov, J. Jersch, S. O. Demokritov, K. Rott, P. Krzysteczko, and G. Reiss, “Transformation of propagating spin-wave modes in microscopic waveguides with variable width,” *Phys. Rev. B* **79**, 054417 (2009).

- <sup>11</sup>O. Wojewoda, T. Hula, L. Flajšman, M. Vaňatka, J. Gloss, J. Holobrádek, M. Staňo, S. Stienen, L. Körber, K. Schultheiss, M. Schmid, H. Schultheiss, and M. Urbánek, “Propagation of spin waves through a Néel domain wall,” *Appl. Phys. Lett.* **117**, 022405 (2020).
- <sup>12</sup>I. Turčan, L. Flajšman, O. Wojewoda, V. Roučka, O. Man, and M. Urbánek, “Spin wave propagation in corrugated waveguides,” *Appl. Phys. Lett.* **118**, 092405 (2021).
- <sup>13</sup>A. V. Sadovnikov, C. S. Davies, V. V. Kruglyak, D. V. Romanenko, S. V. Grishin, E. N. Beginin, Y. P. Sharaevskii, and S. A. Nikitov, “Spin wave propagation in a uniformly biased curved magnonic waveguide,” *Phys. Rev. B* **96**, 060401 (2017).
- <sup>14</sup>H. Qin, R. B. Holländer, L. Flajšman, F. Hermann, R. Dreyer, G. Woltersdorf, and S. van Dijken, “Nanoscale magnonic Fabry-Pérot resonator for low-loss spin-wave manipulation,” *Nat. Commun.* **12**, 2293 (2021).
- <sup>15</sup>A. A. Serga, T. Schneider, B. Hillebrands, S. O. Demokritov, and M. P. Kostylev, “Phase-sensitive Brillouin light scattering spectroscopy from spin-wave packets,” *Appl. Phys. Lett.* **89**, 063506 (2006).
- <sup>16</sup>K. Vogt, H. Schultheiss, S. J. Hermsdoerfer, P. Pirro, A. A. Serga, and B. Hillebrands, “All-optical detection of phase fronts of propagating spin waves in a Ni<sub>81</sub>Fe<sub>19</sub> microstripe,” *Appl. Phys. Lett.* **95**, 182508 (2009).
- <sup>17</sup>C. Dubs, O. Surzhenko, R. Linke, A. Danilewsky, U. Brückner, and J. Dellith, “Sub-micrometer yttrium iron garnet LPE films with low ferromagnetic resonance losses,” *J. Phys. D* **50**, 204005 (2017).
- <sup>18</sup>H. Qin, S. J. Hämäläinen, and S. Van Dijken, “Exchange-torque-induced excitation of perpendicular standing spin waves in nanometer-thick YIG films,” *Sci. Rep.* **8**, 5755 (2018).
- <sup>19</sup>S. O. Demokritov, V. E. Demidov, O. Dzyapko, G. A. Melkov, A. A. Serga, B. Hillebrands, and A. N. Slavin, “Bose-Einstein condensation of quasi-equilibrium magnons at room temperature under pumping,” *Nature* **443**, 430–433 (2006).
- <sup>20</sup>O. Wojewoda, F. Ligmajer, J. Klíma, M. Dhankhar, K. Davídková, M. Staňo, J. Holobrádek, T. Šikola, and M. Urbánek, “Observing high-k magnons with Mie-resonance-enhanced Brillouin light scattering,” [arXiv:2206.05178](https://arxiv.org/abs/2206.05178) (2022).
- <sup>21</sup>M. Vaňatka, K. Szulc, O. Wojewoda, C. Dubs, A. V. Chumak, M. Krawczyk, O. V. Dobrovolskiy, J. W. Klos, and M. Urbánek, “Spin-wave dispersion measurement by variable-gap propagating spin-wave spectroscopy,” *Phys. Rev. Appl.* **16**, 054033 (2021).
- <sup>22</sup>I. Bertelli, J. J. Carmiggelt, T. Yu, B. G. Simon, C. C. Pothoven, G. E. W. Bauer, Y. M. Blanter, J. Aarts, and T. van der Sar, “Magnetic resonance imaging of spin-wave transport and interference in a magnetic insulator,” *Sci. Adv.* **6**, eabd3556 (2020).
- <sup>23</sup>Y. Shiota, S. Funada, R. Hisatomi, T. Moriyama, and T. Ono, “Imaging of caustic-like spin wave beams using optical heterodyne detection,” *Appl. Phys. Lett.* **116**, 192411 (2020).
- <sup>24</sup>B. Heinz, T. Brächer, M. Schneider, Q. Wang, B. Lägel, A. M. Friedel, D. Breitbach, S. Steinert, T. Meyer, M. Kewenig, C. Dubs, P. Pirro, and A. V. Chumak, “Propagation of spin-wave packets in individual nanosized yttrium iron garnet magnonic conduits,” *Nano Lett.* **20**, 4220–4227 (2020).
- <sup>25</sup>L. Flajšman, K. Wagner, M. Vaňatka, J. Gloss, V. Křížáková, M. Schmid, H. Schultheiss, and M. Urbánek, “Zero-field propagation of spin waves in waveguides prepared by focused ion beam direct writing,” *Phys. Rev. B* **101**, 014436 (2020).
- <sup>26</sup>B. A. Kalinikos and A. N. Slavin, “Theory of dipole-exchange spin wave spectrum for ferromagnetic films with mixed exchange boundary conditions,” *J. Phys. C* **19**, 7013–7033 (1986).